Biomed Microdevices (2017) 19:16
DOI 10.1007/s10544-017-0159-2

Optimized acoustic biochip integrated with microfluidics for biomarkers detection in molecular diagnostics

G. Papadakis[1] · J. M. Friedt[2,3] · M. Eck[4] · D. Rabus[3] · G. Jobst[4] · E. Gizeli[1,5]

Abstract The development of integrated platforms incorporating an acoustic device as the detection element requires addressing simultaneously several challenges of technological and scientific nature. The present work was focused on the design of a microfluidic module, which, combined with a dual or array type Love wave acoustic chip could be applied to biomedical applications and molecular diagnostics. Based on a systematic study we optimized the mechanics of the flow cell attachment and the sealing material so that fluidic interfacing/encapsulation would impose minimal losses to the acoustic wave. We have also investigated combinations of operating frequencies with waveguide materials and thicknesses for maximum sensitivity during the detection of protein and DNA biomarkers. Within our investigations neutravidin was used as a model protein biomarker and unpurified PCR amplified *Salmonella* DNA as the model genetic target. Our results clearly indicate the need for experimental verification of the optimum engineering and analytical parameters, in order to develop commercially viable systems for integrated analysis. The good reproducibility of the signal together with the ability of the array biochip to detect multiple samples hold promise for the future use of the integrated system in a Lab-on-a-Chip platform for application to molecular diagnostics.

Keywords Biosensor · Love wave device · Acoustic array · Microfluidics · Molecular diagnostics · Lab-on-a-Chip

1 Introduction

Surface Acoustic Wave (SAW) devices are becoming increasingly significant in bioanalytical sciences (Gronewold 2007; Länge et al. 2008; Voiculescu and Nordin 2012). Their planar geometry has the potential to be combined with other microsystems and components for the development of integrated platforms. The latter, also referred to as Lab-on-a-Chip (LOC), are fast, low cost, portable and easy to operate systems; for these reasons they are promising candidates for environmental analysis, food safety control and point-of care diagnosis (Ahmed et al. 2014; Chin et al. 2012; Wu et al. 2016). A key challenge towards the development of LOC systems is sample transportation and manipulation within the various modules; this is currently achieved thanks to microfluidics technologies, which allow the effective handling of very low sample volumes in an automated manner.

SAW devices have been used as the sensing element predominantly when supporting a Love wave (Gizeli et al. 1992; Kovacs et al. 1994). In such a configuration, the device employs a set of interdigitated transducers (IDTs) to generate and detect a shear horizontal (SH) wave; the utilization of a specific piezoelectric crystal cut gives rise to a SH acoustic wave. In addition, for Love wave operation, a dielectric film is applied on the surface where the IDTs are deposited, covering

✉ G. Papadakis
gpapadak@imbb.forth.gr

✉ E. Gizeli
gizeli@imbb.forth.gr

[1] Institute of Molecular Biology and Biotechnology-FORTH, 100 N. Plastira Str, 70013 Heraklion, Greece

[2] FEMTO-ST Time & Frequency/SENSeOR, 26 rue de l'Epitaphe, 25000 Besançon, France

[3] SENSeOR SAS, Temis Innovation, 18 rue Alain Savary, 25000 Besançon, France

[4] Jobst Technologies GmbH, Engesserstraße 4b, 79108 Freiburg, Germany

[5] Department of Biology, University of Crete, 71409 Vassilika Vouton, Greece

Published online: 29 March 2017

both the sensing area and IDTs. The film acts as a waveguiding layer when the shear acoustic velocity in the film is lower than in the piezoelectric substrate. In practice, film deposition results in high energy confinement and, consequently, increased sensitivity at the film/liquid interface (Gizeli et al. 1992). Optimized layer thicknesses can vary from several micrometers (i.e. around 5 μm at 150 MHz) in the case of stiff materials (i.e. silica, V_{shear} = 3000 m/s) to few micrometers (i.e. around 1 μm) in the case of soft ones (i.e. photoresist or PMMA, V_{shear} ~ 1000 m/s). It should be noted that polymer overlayers can be applied using simple (spin coating) and inexpensive procedures in terms of both material and processing cost; for this reason they are very attractive for mass production (Rasmusson and Gizeli 2001). In addition, polymer-based guiding layers allow multiple use of the SAW devices after removal by acetone rinsing and re-deposition of the film, without compromising the Love wave sensor sensitivity or performance.

Love wave sensors have been used in bioanalytical and diagnostic applications for detecting mainly three kinds of targets: protein biomarkers, genetic biomarkers, and whole cells. The detection of protein biomarkers forms the largest pool of Love wave sensors applications; these are mainly label-free assays, as reported during the detection of analytes such as cardiac markers (Mitsakakis and Gizeli 2011a), interleukin (Krishnamoorthy et al. 2008), thrombin (Perpeet et al. 2006) and antibodies (Josse et al. 2001; Saha et al. 2003). In all the above works, the typical dynamic concentration range of protein biomarkers lies in the nM range and includes proteins within a wide spectrum of molecular weights from thrombin (36 kDa) (Perpeet et al. 2006) to pregnancy associated plasma protein A (540 kDa) (Saha et al. 2003) for devices operating at around 150 MHz. Higher sensitivities in the pM range have been reported when a sandwich immunoassay was combined with a gold staining mass-enhancement step and Love wave devices operating at 200 and 400 MHz (Lee et al. 2011). Love wave sensors for cell and DNA detection have also attracted some attention, namely in the detection of bacteria (Matatagui et al. 2013; Tamarin et al. 2003), bacterial biofilms (Kim et al. 2016), cancer cells (Bröker et al. 2012) and single mutations in gene fragments (Gronewold et al. 2006).

While the above works leave no doubt of the analytical potential of Love wave sensors, the main challenges for their application in commercial diagnostic LOC platforms are related to improving their sensitivity and reproducibility as well as their effective integration with the fluidics module. Acoustic sensors, unlike optical ones, respond to a number of changes occurring at the device surface/liquid interface, namely deposited mass (including both elastic and inelastic soft matter) and viscosity and electrical properties of the sample solution. This plethora of information is depicted in the two signals, which are related to acoustic wave propagation: the phase or frequency and the amplitude. Data shown by Länge and Rapp (Länge and Rapp 2009) suggest that viscoelastic changes accompanying protein adsorption occurring in 3D or 2D hydrogels are not necessarily analogous to each other, indicating the necessity for developing experimental protocols and mathematical tools for obtaining reliable and reproducible signals. A common approach to overcome this problem has been the application of a reference channel for calibrating phase or frequency response (Lee et al. 2013). In addition, it has been generally accepted that phase measurements are analogous to the amount of deposited mass; for this reason, phase or frequency measurements are reported in the majority of the published works concerning Love wave biosensors. Recently, this concept has been proven experimentally, when a linear correlation between protein mass (measured by SPR) and phase change was obtained for different proteins and attachment methods (Mitsakakis et al. 2014; Saha et al. 2003). An alternative and rather revolutionary concept refers to employing both acoustic signals for probing intrinsic properties of the attached biomarkers, namely their conformation. This is achieved by monitoring the ratio of amplitude change versus phase change (i.e. $\Delta A/\Delta Ph$), thus, calibrating energy losses to the amount of deposited mass. This ratio has been shown both theoretically and experimentally to reflect on the shape and size of biomolecules (Papadakis et al. 2009, 2012; Tsortos et al. 2008, 2015, 2016). The analytical value of this approach as opposed to the phase measurement alone, has been illustrated with great success in nucleic acid biomarkers detection, namely, breast cancer biomarkers, plant pathogens and also during single nucleotide polymorphism detection in mosquitoes (Papadakis et al. 2013, 2015; Papadakis and Gizeli 2014). Still, it is not yet entirely clear which signal should be preferentially monitored during protein and DNA detection.

Moreover, the application of SAW devices in LOC platforms requires, ideally, the fabrication of array biochips for multiple analysis integrated with an efficient fluidics module. The latter sets an engineering challenge due to the Love wave devices' high sensitivity to surface perturbations, including the application of external pressure as a result of flow cell attachment. This is primarily important in the case of a quartz piezoelectric substrate, since, quartz acoustic devices cannot operate with the IDTs immerged in liquid, and require the use of a flow cell for liquid-confinement between the input and output IDTs. Generally, and for research purposes, simple flow cell designs are attached to the sensors surface by employing a gasket and a sufficient external pressure to achieve sealing. More sophisticated approaches have been employed where a microfluidic channel was applied on a SAW resonator (instead of Love wave delay line) (Länge et al. 2006) or a microfluidic-on-SAW (μf-on-SAW) module was combined with a Love wave device to produce four sensing channels during protein biomarkers detection (Mitsakakis et al. 2008; Mitsakakis and Gizeli 2011b). A SAW array-type chip, operating in a Love wave mode and consisting of 5 sensors was described by Perpeet et al. (Perpeet

et al. 2006) for thrombin analysis. Finally, recent publications described a point-of-care testing system, where a dual Love wave device was employed in a centrifugally actuated LOC platform for cardiac troponin detection (Lee et al. 2013); a bacteriophages-testing Love-wave immunosensor combined with microfluidics (Matatagui et al. 2013); and, a Love wave sensor combined with microfluidics for biological warfare agents detection (Matatagui et al. 2014). Despite of the above few works, the application of acoustic sensors in LOC platforms as the biosensing element is still in its infancy, even though the system exhibits high mass sensitivity and is relatively simple to fabricate. It is our opinion that difficulties related to the SAW device integration with the fluidics and the device high sensitivity to several parameters and sensing mechanisms are the main reason for this observation.

The motivation of this work is to perform a systematic study of Love wave biosensors by taking into account all the parameters that affect their performance, namely, operating frequency, microfluidic module and type of target analyte and sample. The final goal is to select the best device and detection protocol that could form the basis of a viable commercial system for biomarkers detection. For this reason, the work is focused on the fabrication of a dual and array type Love wave devices and their combination with a microfluidic module that results in minimum signal distortion. In addition, the dual device was fabricated to operate at two frequencies, 155 and 300 MHz. Optimization of the flow cell sealing material and contact area was carried out in order to produce a fluidic design, which - combined with a Love wave array chip - would allow for the detection of 12 samples. Finally, the sensitivity of the phase and amplitude acoustic signals, as well as their combined use in the form of the acoustic ratio, was evaluated during the detection of protein and nucleic biomarkers, both of interest in molecular diagnostics. To our knowledge, this is the first time that all these parameters are tested in parallel, placing also emphasis on the effect of the type and size of the target analyte to the acoustic signal response.

2 Materials and methods

2.1 Fabrication of SAW devices in a dual and array-type configuration operating at 155 & 300 MHz

Love-mode dual SAW sensors were fabricated on a ST quartz (YXI/36°) substrate by first patterning 150 nm thick aluminium electrodes following a split-finger geometry resulting in a 32 μm acoustic wavelength and a 8 μm electrode period, with a metallization ratio of 50%, for the 155 MHz devices. Devices operating at 300 MHz were also manufactured following a similar process; in this case the acoustic wavelength and electrode period were 16 and 4 μm, respectively. Both dual SAW delay line devices had an overall size of 16 × 24 mm (Fig. 1a). A waveguiding layer was formed by using photoresist or PMMA; S1805 photoresist (Shipley, U.S.) guiding layer (~1 μm thick) was obtained by spin coating (Specialty Coating Systems, INC, Spincoater P6700 series) at 850 rpm and for 30 s S1805; various concentrations of PMMA (Aldrich, Milwaukee, WI), i.e., 8, 17, 20% (*w*/w) in ethoxyethyl acetate (Aldrich, Milwaukee, WI), spin coated at 4000 rpm for 4 min, were used to form layers of 0.35, 0.8 and 1, μm, respectively. In the case of a photoresist guiding layer, a photolithographic step was included for opening the electrical pad access after exposure to UV light. For PMMA, electrical contact areas were cleaned manually by gentle scratching. Typical insertion losses of the fabricated devices in air were in the 25 dB range when measured under a probe station.

For the production of an array SAW chip, a 4-acoustic channel design was produced in which all non-mandatory dimensions were shrunk to maximize the number of chips manufactured on each 4 in. wafer and, hence, minimizing manufacturing cost. The device dimensions were 16 × 16 mm and each device comprises 4 channels (Fig. 1b) instead of two (Fig. 1a). The same fabrication and waveguide film-deposition process was followed as for the dual delay line while the operating frequency was at 155 MHz.

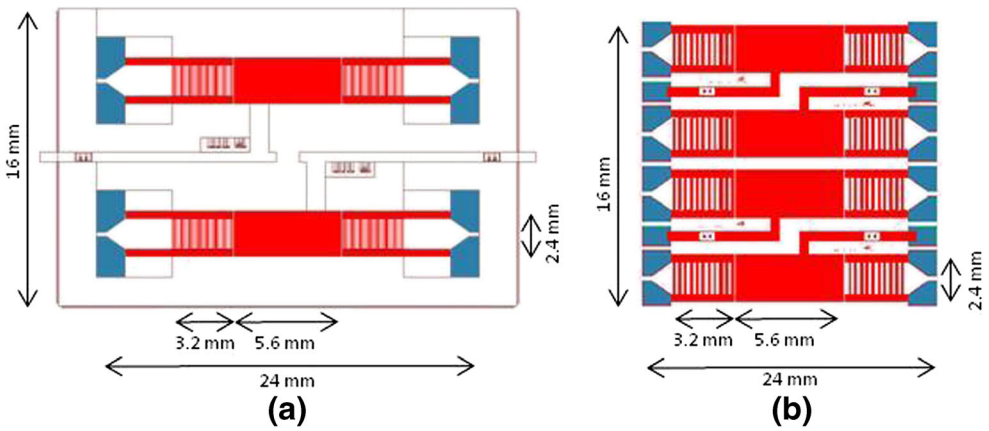

Fig. 1 Sketch of a **a** dual SAW delay line device operating at 155 or 300 MHz, and **b** a SAW array biochip, incorporating 4 sensing channels and operating at 155 MHz

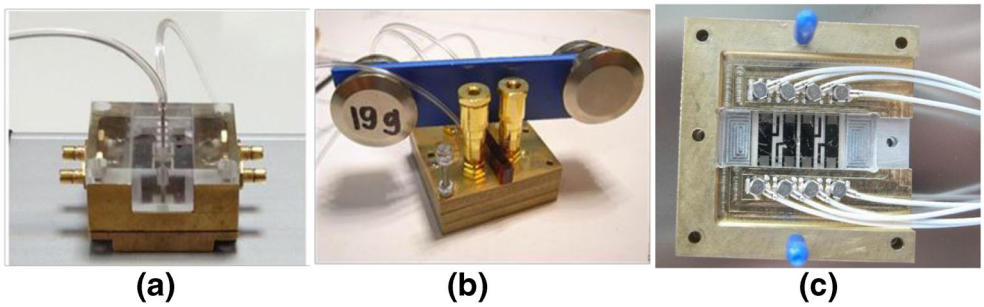

Fig. 2 Photo of Type I **a** and Type II **b** docking station and flow cell for the dual SAW device; **c** Docking station for the SAW array chip

2.2 Design and fabrication of the docking station for the dual and array SAW chips

Two docking stations were manufactured and tested for the two dual SAW devices (155 or 300 MHz). Type I (Fig. 2a) consisted of a brass base with a recess for mounting the device; the top part, also made of brass, had 8 spring probes for enabling the electrical contact between the network analyzer and the device. Electrical contact was realized after bringing the two parts together by using 4 screws placed on the underside of the low base. A Perspex flow cell was placed on top of the device attached to the upper brass holder by using 4 screws; this method provided sealing but without good control of the applied force per screw. To overcome this problem, a second docking station, Type II (Fig. 2b), was manufactured. Here, an even distribution of the applied force on the device surface was achieved by using 4 magnets of 19 g each, enabling the application of a strictly vertically-acting highly stable force onto the PDMS seals.

The third docking station for the array SAW biochip shown in Fig. 2c, also employs a brass base and top part for positioning the device and making electrical contacts, respectively. In this case, the pitch of the contact pads was reduced to the limits of reliable electrical contacting without using wire bonding. For achieving electrical interfacing to the 16 × 16 mm SAW array chip, twelve ground contacts were realized by 350 μm diameter and 3 mm short (minimizing capacitance) spring probes (CCP Contact Probes Co., Ltd., Taipei, Taiwan R.O.C) directly hosted in the brass frame, and eight further spring probes directly in contact with 3 mm pitch surface mount devices high frequency (SMD HF) connectors (Hirose W.FL-R-SMT-1(10), HIROSE ELECTRIC CO., LTD, Tokio, Japan) were utilized. This type of micro coaxial connector is widely used in high frequency consumer devices such as mobile phones. The low-profile (2 mm, when jack and plug are mated) coaxially shielded HF connector cables (GradConn Cable 040 RF, GradCon CO., LTD, Taoyuan, Taiwan R.O.C) provide a SMA socket on the opposite side for connection to the network analyzer."

2.3 Design & fabrication of the fluidics module for the dual and array SAW chips

For the dual SAW delay line, two types of Perspex flow cells (see Fig. 3), with varying geometries of the inserted PDMS based seal - *in situ* casted onto the 2 mm PMMA sheets - were made and tested. Seals with different seal-widths were made from two PDMS materials, i.e. Nusil R-2188 and Nusil MED-6215, with a shore hardness corresponding to 20 and 50 respectively. Note that the shore hardness is a scale of a material's resistance to permanent indentation, and, usually, is determined from the depth a defined body penetrates into the

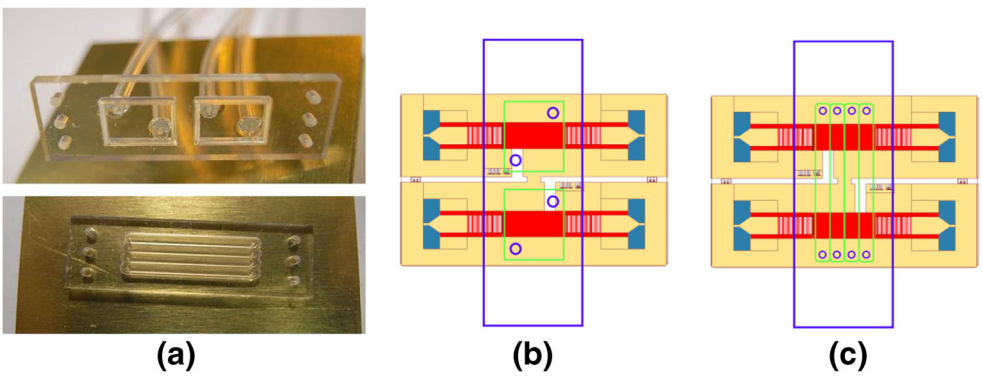

Fig. 3 **a** Photographs of flow cells used for the dual SAW chip incorporating 2 (*top*) and 4 (*bottom*) fluidic channels; **b** schematic of the 2-channel flow cell, where each channel creates a single compartment flow area on top of each sensor; **c** Schematic of the four-channel flow cell setup, which creates a total of 8 channels over the 2 sensors. (PDMS seals represented by *green rectangles*; *blue rings* show the position of the fluidic in- and outlet; the *blue rectangles* indicate the border of the flow cell)

material at a given force. The range of d seal-widths tested in this work corresponded to seals with different number of walls and wall thicknesses; namely: 2 × 0.06 mm = 0.12 mm, 5 × 0.06 mm = 0.3 mm, 8 × 0.06 mm = 0.48 mm, 5 × 0.25 mm = 1.25 mm, and 5 × 0.4 mm = 2 mm.

For the acoustic chip array, a more sophisticated flow assembly was manufactured (see Fig. 4) consisting of a flat fluid connector and the actual flow cell; the former is the part that connects the flow channels to the liquid samples, while the latter is the part that comes in contact with the SAW device surface. The two parts were connected by a Computer Numerical Control (CNC) cut adhesive patch. Figure 4a shows the flow assembly: the flat 240 μm thick flexible fluid connector was made by hot lamination of three layers of CNC patterned polyester foil and comprised flow channels of 80 μm height; the flow cell comprised channels with a pitch of 800 μm and a width of 400 μm. Figure 4d gives a top view of the flow assembly wherein the channels are clearly shown as well as the positioning of the gaskets (blue) and subsequently formed areas for liquid flow. The assembly design-flexibility allowed for the attachment of various flow cell units incorporating different numbers of channels; i.e., 3 microfluidic channels over the 3 sensors and the 4th one used as a reference (shown in Fig. 4d), or 1–4 microfluidic channels going all over the 4 sensors. All fluid connections were placed at the same side of the assembly (left in Fig. 4a, d) in order to have a simple access to all fluid interconnects at the same location. This fluid connector was terminated by the fluid break out (Fig. 4b) comprising a staggered tube terminal, which allowed connecting a total of 8 standard 2.4 mm outer diameter tubes at just 1.6 mm channel outlet pitch – a demonstration of high density LOC to external fluidics connectivity. Figure 4c shows the flow assembly placed onto the SAW chip in the SAW docking station. The red plastic gantry construction is hosting two springs that apply a constant force (adjustable by the two screws on top) onto the flow cell connector that presses the flow cells seal onto the SAW chip. Built height and construction were experimentally chosen to allow optimisation of the applied force by adjusting the screw position and controlling the SAW response to minimize the losses while still obtaining a leak free sealing.

2.4 Acoustic detection of protein and DNA binding assays

SAW devices (dual delay lines and biochips) were etched prior to measurements using an air Plasma Cleaner/Sterilizer PDC-002 (Harrick Plasma Inc., Ithaca, NY, USA) instrument for 150 s at high RF level. Acoustic experiments were carried out in continuous flow where PBS running buffer and samples were exchanging in an alternating manner. Physical adsorption of neutravidin (Invitrogen, A2666) was monitored by injecting 200 μl of a 200 μg/mL solution under constant flow of 20 μl/min. Acoustic data was monitored in real time as changes in amplitude (ΔA) and phase (ΔPh) of the acoustic wave, which were also used for the calculation of the acoustic ratios (ΔA/ΔPh (dB/deg)).

DNA amplicons (GenBank NC_003197.2) were produced from *Salmonella* Typhimurium genomic DNA (kindly provided by Pasteur Institute, Paris, France) in PCR reactions using the Hotstart polymerase kit (KAPA Biosystems Inc., Wilmington, MA, USA) and following the manufacturer instructions. 2.5 pmoles of the forward and reverse primers were included in each amplification reaction. The reactions were conducted with a PeqStar 2× (Peqlab Biotechnologie GmbH, Erlangen, Germany)

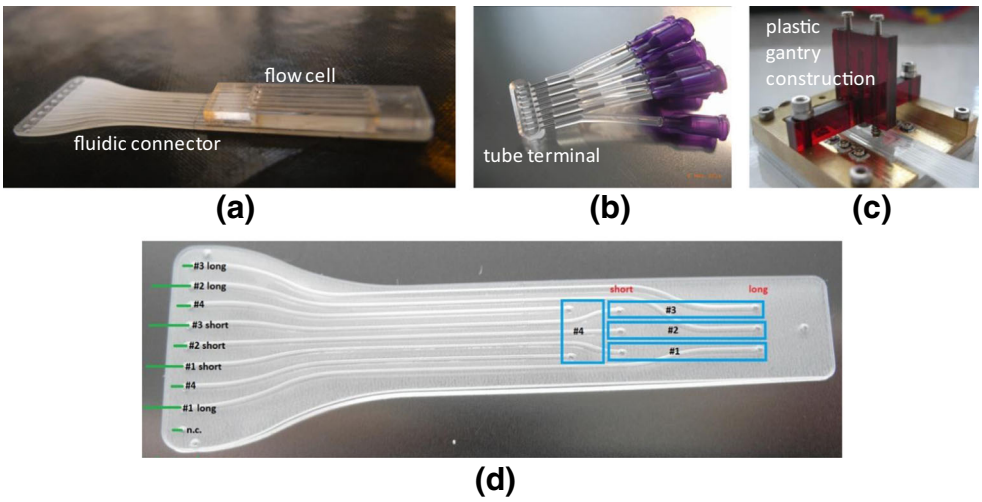

Fig. 4 **a** Four channel flow cell with attached fluidic connector. **b** Tube terminal for accessing the fluidic module. **c** Picture of SAW docking station (same to that shown in Fig. 2c) with flow cell placed and engaged; **d** top view of the fluidic assembly shown in **a**; the *blue areas* indicate the positioning of the gasket

thermocycler at 95 °C for 3 min, followed by 40 cycles of 95 °C for 10 s, 62.5 °C for 10 s and 72 °C for 10 s. The final step was at 72 °C for 1 min. The primers used for the 666 bp DNA were: Forward: 5′-Biotin-GAAGCGTTAGTGAGCCGTCTGCG-3′, Reverse: 5′-ATCAGCGACCTTAATATCTTGCCA-3′.

The 86 bp DNA (GenBank M24473) was produced from *Mycoplasma hominis* genomic DNA using the IsoAmp®II tHDA kit (Biohelix, Beverly, MA, USA) for isothermal amplification following the manufacturer instructions. Each reaction was supplemented with 5 pmoles of the: Forward (5′-Biotin-CACTAAAA GATGAGGGTGCGGAACATT-3′). Reverse (5′-AGTC TCTCGACCCGGCTAAACATCATA-3′) primer. The reactions were incubated at 65 °C for 1 h in a thermocycler.

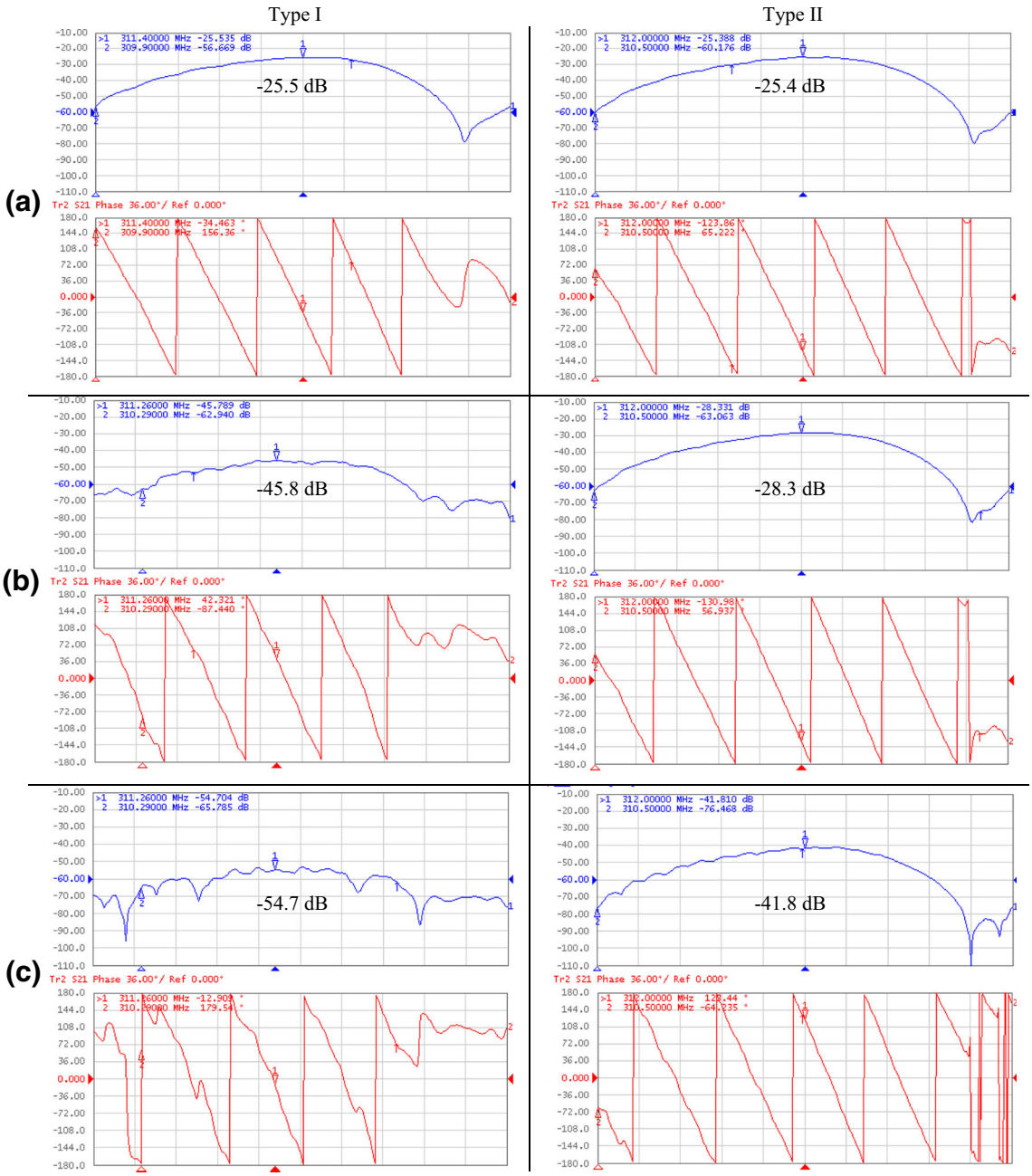

Fig. 5 Images of acoustic signal spectra with flow cell Type I (*left*) and optimized flow cell Type II (*right*), both used on the 300 MHz device. From top to bottom: **a** Signal in air without flow cell, **b** signal in air with the flow cell, **c** signal with liquid filling the flow cell. The x axis represents a 3 MHz frequency span with marker 1 positioned at the central frequency. The y axis shows amplitude (dB) (*blue*) and phase (deg) values (*red*)

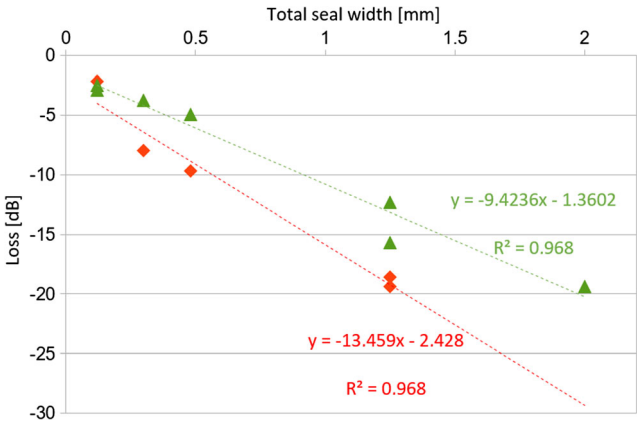

Fig. 6 Testing results of various flow cells and seal materials plotted as loss vs total wall width; *red*: PDMS with shore hardness of 50; *green*: PDMS with shore hardness of 20. Tests were performed in air using the setup presented in Fig. 2b and the flow cells in Fig. 3a. The total seal width corresponds to the sum of all seal wall thicknesses along the delay line

3 Results and discussion

3.1 Optimized flow cell for minimum acoustic losses

Interfacing of the SAW with other modules in a LOC platform poses the challenge of achieving fluidic connection with minimal losses to the acoustic wave. Excess of acoustic losses can significantly affect the sensor response in terms of the signal to noise ratio and, hence, detection limit. With respect to this point and in order to allow for a careful investigation of the influence of the flow cell on the SAW signal, two types of docking stations were fabricated and tested. The first one (Type I, see Fig. 2a) provided good sealing but offered no means for controlling the applied force on each screw, resulting in an uneven force distribution and possibly application of an unnecessarily high force. This is depicted in Fig. 5 (left), where the corresponding spectrum obtained when the 300 MHz device was in contact with the liquid sample was poor, resulting in 20 dB losses associated with the fluidic gasket adherence to the SAW sensor (Fig. 5b). Figure 5 (right) shows that the Type II flow cell setup results in a significant improvement of the acoustic spectrum for the same device, adding as little as 1–3 dB extra losses as a result of the fluidic gasket placement on the acoustic path. Apparently, the construction of a system enabling the application of a very well centered, stable and controlled force to the flow cell resulted in much better acoustic signal response.

To further improve the flow cell design, a systematic study with respect to the gasket geometry and material used was carried out. Based on Fig. 5, flow cell Type II was constructed and combined with flow cell geometries incorporating PDMS seals of various width and hardness. After placing each flow cell on the device surface, the effect of each gasket geometry on the insertion loss of the SAW device was measured. According to Fig. 6, losses scale up linearly with the total width of the PDMS in contact over the acoustic path. In addition, a significant distinction in the losses depending on the shore hardness was found for two of the PDMS materials (hardness 50 and 20 respectively). This can be explained by a collapse of the narrow portion of the seal in contact with the SAW chip, leading to an increased material load to the SAW chip surface that generates excess losses. These experiments suggest that macroscopic material properties influence the losses of the SAW device in an extent that may add over 40% of additional insertion loss (for the herein compared shore hardness of 20 and 50 up to 10 dB extra loss for the same contact area). The above experiments allow one to suggest as a general rule to use flow cell seals, which are as narrow as possible and made from a soft material, keeping in mind that the additional deformation occurring for softer materials may also increase the contact area.

3.2 Evaluation of the dual love wave device to protein binding as a function of the operating frequency

The performance of the two delay lines, operating at 155 and 300 MHz, was evaluated in terms of their sensitivity to protein adsorption by using the optimised flow cell system shown in the previous section (Type II and Nusil R-2188 PDMS-shore hardness 20). The effect of the waveguiding layer on phase and amplitude change is well known, and has been documented by many researchers (Du et al. 1996; Gizeli 1997; McHale et al. 2002). Here, we compared the devices' response during

Table 1 Phase (ΔPh) and amplitude (ΔA) change, respectively, of the Love wave sensor during the direct adsorption of 200 μg/ml neutravidin on the photoresist guiding layer; results are shown for the dual 155 and 300 MHz wave devices

Device freq. (MHz)	Waveguide	ΔA (dB)	ΔPh (deg)	ΔA/ΔPh (dB/deg)
300	Photoresist 0.4 μm	2.25 ± 0.75	47.5 ± 12.5	0.047 ± 0.003
300	PMMA 0.17 μm	2.5 ± 0.5	29	0.086 ± 0.017
300	–	<1	<5	<0.2
155	Photoresist 1 μm	1.5	32.5 ± 2.5	0.046 ± 0.003
155	PMMA 0.77 μm	1.25 ± 0.25	20 ± 5	0.069 ± 0.009
155	PMMA 0.17 μm	1.5 ± 0.5	7.5 ± 2.5	0.2
155	–	<1	10	<0.1

Table 2 Comparison of acoustic ratios calculated for amplification reactions producing DNA fragments of 2 different lengths and at 2 different operating frequencies; $(AR)_s$ and $(AR)_c$ correspond to the acoustic ratio obtained from the amplification samples and control solutions, respectively

DNA #b	Operating Frequency (MHz)	(AR)s (dB/deg)	(AR)c (dB/deg)
666	300	0.243 ± 0.056	0.185 ± 0.027
666	155	0.218 ± 0.003	0.069 ± 0.006
86	300	0.052 ± 0.007	0.035 ± 0.012
86	155	0. 130 ± 0.043	0.080 ± 0.016

Each experiment was conducted 3 times

the deposition of neutravidin on Love wave devices employing various thicknesses of photoresist or PMMA as waveguiding layer. The thicknesses of the guiding layers were chosen to be close to the optimum for each one of the 2 frequencies (0.4–0.17 μm for the 300 MHz and 1–0.77 μm for the 155MHZ). The 0.17 μm thickness was also used with the 155 MHz device for comparison purposes with the 300 MHz device. In all cases, it was observed that phase and amplitude sensitivity to protein adsorption increased with increasing the waveguide thickness. The largest phase change was observed with the 300 MHz device employing a 0.4 μm photoresist guiding layer, followed by the 155 MHz device, employing a 1 μm photoresist guiding layer. Table 1 shows that the mass-sensitive phase response increases significantly with increasing the frequency and waveguide thickness, while the amplitude and acoustic ratio are less affected and for this reason were not considered appropriate to be used for monitoring protein detection. It should be noted that when higher waveguide thicknesses than those shown in Table 1 were employed, the signal of both devices was damped.

3.3 Evaluation of the dual love wave sensor to DNA detection as a function of the operating frequency

In a second round of evaluation, the sensitivity of each of the two operating frequencies was investigated for those applications including the detection of genetic biomarkers. For this purpose, the two most sensitive Love wave geometries shown in Table 2 (i.e., 300 MHz with 0.4 μm photoresist and 155 MHz with 1 μm photoresist) were used to detect the presence of a target-DNA after PCR amplification. For the binding of the target molecules to the surface, double stranded DNA amplicons with a biotin molecule at the 5′ end were produced using PCR in combination with a neutravidin-coated Love wave device (Fig. 7). Specifically, genomic DNA was amplified, producing DNA molecules of 666 or 86 bp in length; the amplification solutions were loaded without prior purification on both the 300 MHz and 155 MHz devices, and in each case the phase and amplitude of the wave were monitored in real time. PCR reactions without DNA were also used as a control; in this case, any response obtained from the control sample would be related to the non-specific binding of the enzymes and primers present in the amplification mixture (Fig. 7).

Previous results from our group have shown that the acoustic ratio is more specific and sensitive to DNA binding through a biotin to the neutravidin surface than each signal alone (Papadakis et al. 2013; Papadakis and Gizeli 2014); for this reason we calculated the corresponding acoustic ratios) for the sample (AR_s) and control (AR_c) solutions using the two devices. As expected (Papadakis and Gizeli 2014), positive amplification reactions resulted in higher acoustic ratio values (Table 2) due to the presence and binding of the biotinylated target DNA. This was true for both the 155 and the

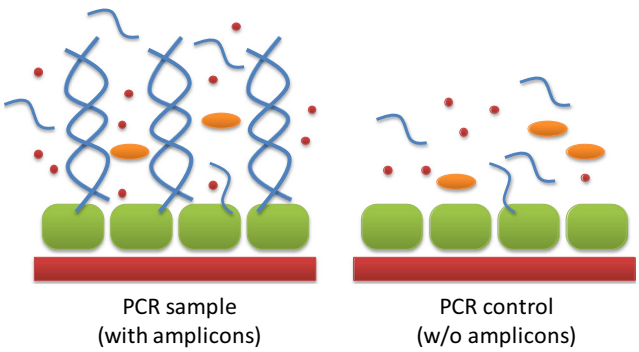

Fig. 7 Schematic for the detection of the presence of amplified DNA targets (*blue*) immobilized on a neutravidin layer (*green*). A negative amplification reaction without DNA template but containing primers (*blue short curved lines*), enzymes (*orange*), dNTPs (*red circles*) etc. is used as a control

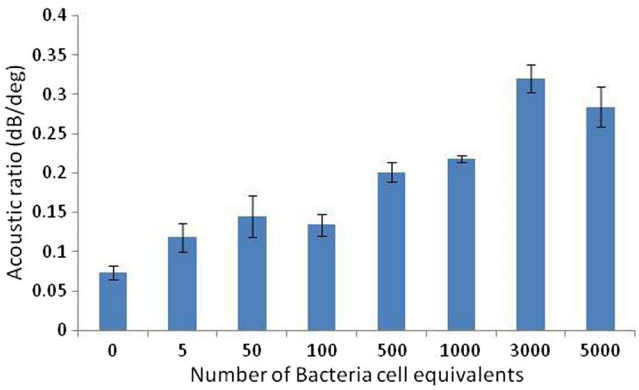

Fig. 8 Acoustic ratio measured for PCR samples varying in the starting amount of bacteria cell equivalents as template. Experiments were performed in at least triplicates

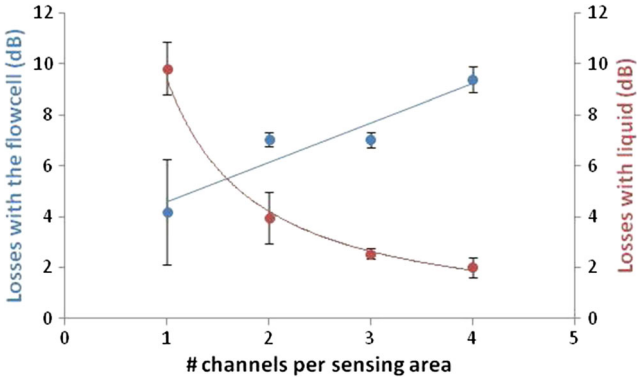

Fig. 9 Acoustic signal losses monitored upon placement of the different flow cells in air (*blue*) and additional losses caused by liquid flow through one of the channels (*red*). Each measurement was conducted in triplicates

300 MHz devices and the two DNA targets. However, for the implementation of the acoustic DNA assay to applications of commercial interest, it is important that $AR_s >> AR_c$. According to Table 2, in the case of the 666 bp target, the acoustic ratio difference favors the use of a low frequency device ($[AR_s/AR_c]^{155} = 3.2$, while $[AR_s/AR_c]^{300} = 1.3$). Interestingly, in the case of the shorter 86 bp DNA target, there is no significant difference between the two ARs obtained with the two devices. Several reasons may account for this observation, i.e., the effect of viscoelastic losses which change significantly with the operating frequency or type of biofilm formed with each control sample; further experiments are necessary in order to elucidate the basis of this observation. Furthermore, it was concluded that, contrary to the observed mass-sensitivity increase during protein adsorption, higher operating frequencies do not offer any significant advantage towards DNA detection based on the acoustic ratio method and under the current experimental conditions.

Moreover, we used the 155 MHz photoresist coated Love wave sensor to check the detection limit for *Salmonella*, i.e., the minimum number of initial pathogens, expressed as Bacteria Cell Equivalents – BCE (Hein et al. 2006), which can be detected after amplification. For this reason, BCE dilutions equivalent to 0, 5, 50, 100, 500, 1000, 3000 and 5000 cells were prepared and tested after PCR. Each experiment was conducted in triplicates and the results are summarized in Fig. 8. Note that as mentioned in Section 3.3, here also the samples are loaded straight after the PCR and without any prior purification. Acoustic data indicate clearly the ability of the acoustic sensor to detect PCR amplicons derived from as little as 5 BCE. Although it does not seem possible to discriminate 5 from 50 or even 100 BCE due to the PCR inherent variability, there is a clear trend where acoustic ratio increases as the starting amount of template increases up to 5000 BCE.

3.4 Evaluation of the integrated love wave array biochip with microfluidics for multi-sample analysis

Love wave array biochips operating at 155 MHz with optimized photoresist layer were fabricated and tested in terms of acoustic signal losses resulting from flow cell attachment and subsequent liquid loading. Signal evaluation was performed by using four different flow cell geometries on top of the array

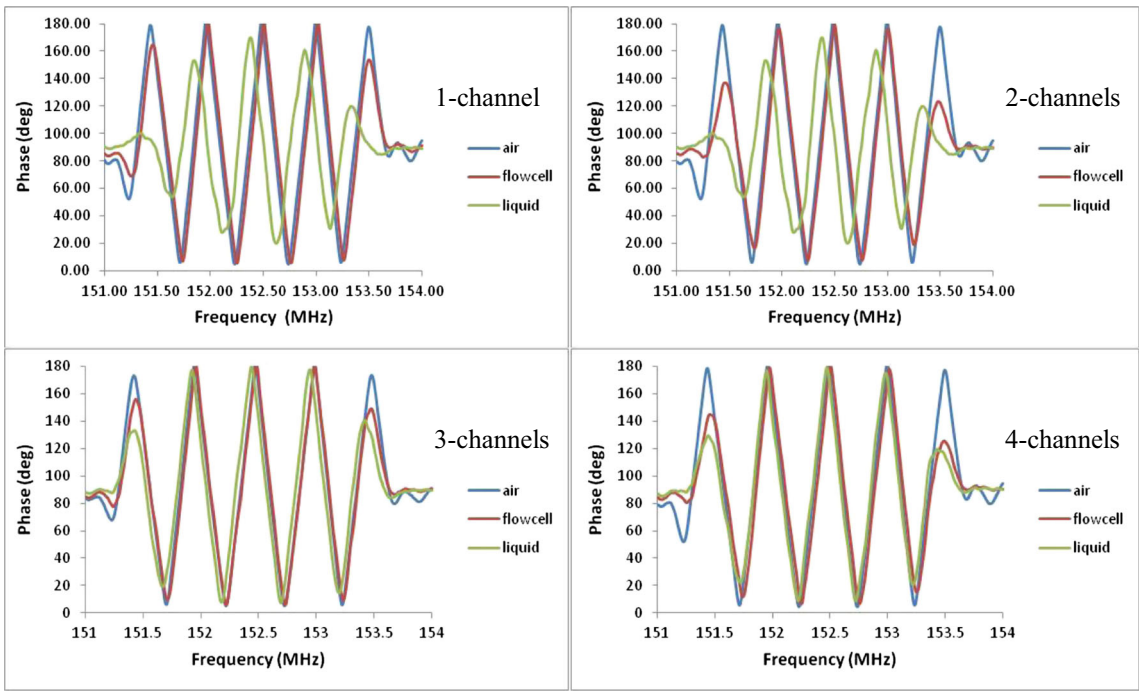

Fig. 10 Acoustic signal evolution from air to liquid for one sensing area using the four different flow cells

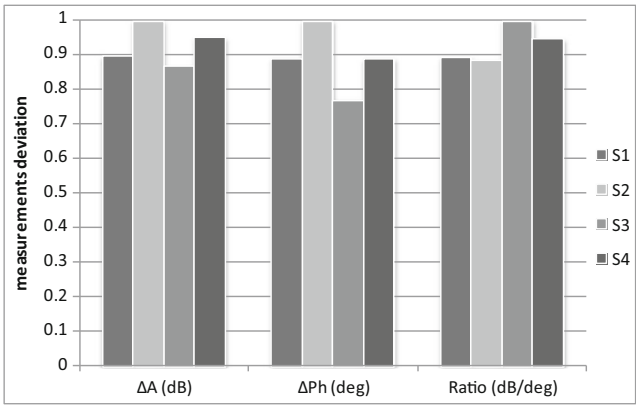

Fig. 11 Deviation of the Δphase, Δamplitude and acoustic ratio recorded with unpurified *Salmonella* DNA amplicons on each sensing area of a biochip. The values are normalized in respect to the maximum measured value

biochip, which divided the sensing areas into 1, 2, 3 and 4 parts, respectively. The 1-channel and 4-channel geometry per sensing area is depicted in Fig. 3. The tests showed that as the number of channels increases from 1 to 4, the losses in air due to the flow cell also increase from 4 up to 9 dB. When liquid flowed through each one of the channels it caused an additional increase in losses from 2 dB (for the 4-channel flow cell) up to almost 10 dB (for the one-channel flow cell) (Fig. 9). Overall, the total losses ($Losses_{seal}$ + $Losses_{liquid}$) for one channel observed when increasing the number of flow cells from 1 to 4 varies from 14 dB (one channel) to 11 dB (4 channels), with the minimum total losses being 9 dB for the 3-channel system. It should be noted that there is no obvious physical relationship between the two plots shown in Fig. 9, since the red one is related to damping caused by liquid placed in an area of particular dimensions while the blue one to damping caused by increasing the number of contact points between the gasket and the device surface. Interestingly, despite the observed losses, the desirable linearity in the phase signal is still maintained (Fig. 10), probably thanks to the use of the optimized flow cell assembly system. The linearity of the phase response is of high significance in acoustic sensing since it determines by large the reproducibility and reliability of the measurement (Ballantine et al. 1996).

The biochip evaluation for biomarker detection in terms of the reproducibility of the signal was further carried out by performing measurements with the 3-channel microfluidic assembly on the biochip array. In agreement with previous studies (Mitsakakis and Gizeli 2011a), the system's response during protein (neutravidin) detection was found to result in a reproducibility which was better than 90% between the different microfluidic channels (data not shown). The biochip evaluation was finally completed by performing measurements with amplified *Salmonella* genomic DNA (666 bp), as described in Section 3.3. Results are summarized in Fig. 11 where, a reproducibility ranging from 87% to 95% for amplitude, 77% to 89% for phase and 88% to 95% for acoustic ratio was observed between the measured values from the 4 sensing areas. However, it should be noted that the larger variation observed with the DNA samples is mainly due to the fact that this analysis was performed in complex samples.

4 Conclusions

The current work shows that the development of acoustic assays for real world applications requires the parallel assessment of multiple parameters of a mechanical and analytical nature, namely the device operating frequency, flow cell geometry and integration, employed analytical protocol, nature and size of the target analyte and type of the sample (pure versus complex). Our results clearly indicate the need to verify all these parameters experimentally in an individual as well as combined way. This is clearly shown in the case of the operating frequency and target analyte: protein detection through phase monitoring was found to depend on the operating frequency and increase with it. In the case of DNA detection, through, acoustic ratio monitoring showed that the optimum operating frequency is strongly related to the size of the target DNA molecule with low frequency devices being the best candidates for DNA sensing. In addition, the use of unpurified PCR or isothermal amplification samples in the case of DNA analysis points out towards the need for low operating frequencies when complex samples are analysed. Overall, the demonstrated optimized fluidic design with the Love wave array chip holds promise for further integration with other modules for creating Lab-on-a-Chip platforms allowing the efficient and sensitive detection of both protein and DNA targets.

Acknowledgements The authors would like to acknowledge the financial support of the European Commission through FP7-ICT-2011.3.2 (LOVE-FOOD, No 317742) and HORIZON2020-ICT 28-2015 (LoveFood2Market, No 687681) grants.

References

M.U. Ahmed, I. Saaem, P.C. Wu, A.S. Brown, Crit. Rev. Biotechnol. **34**, 180–196 (2014)

D. Ballantine, Jr., S.J. Martin, A.J. Ricco, G.C. Frye, H. Wohltjen, R.M. White and E.T. Zellers, *Acoustic wave sensors: Theory, design and physico-chemical applications* (Academic Press, San Diego, 1996), p. 436

P. Bröker, K. Lücke, M. Perpeet, T.M.A. Gronewold, Sensors Actuators B Chem. **165**, 1–6 (2012)

C.D. Chin, V. Linder, S.K. Sia, Lab Chip **12**, 2118–2134 (2012)

J. Du, G.L. Harding, J.A. Ogilvy, P.R. Dencher, M. Lake, Sens. Actuators, A **56**, 211–219 (1996)

E. Gizeli, Smart Mater. Struct. **6**, 700–706 (1997)

E. Gizeli, N.J. Goddard, C.R. Lowe, A.C. Stevenson, Sensors Actuators B Chem. **6**, 131–137 (1992)

T.M. Gronewold, Anal. Chim. Acta **603**(2), 119–128 (2007)
T.M. Gronewold, A. Baumgartner, E. Quandt, M. Famulok, Anal. Chem. **78**(14), 4865–4871 (2006)
I. Hein, G. Flenka, M. Krassnig, M. Wagner, J. Microbiol. Methods **66**, 538–547 (2006)
F. Josse, F. Bender, R.W. Carmose, Anal. Chem. **73**(24), 5937–5944 (2001)
Y.W. Kim, M.T. Meyer, A. Berkovich, S. Subramanian, A.A. Iliadis, W.E. Bentley, R. Ghodssi, Sens. Actuators, A **238**, 140–149 (2016)
G. Kovacs, M.J. Vellekoop, R. Haueis, G.W. Lubking, A. Venema, Sens. Actuators, A **43**, 38–43 (1994)
S. Krishnamoorthy, A.A. Iliadis, T. Bei, G.P. Chrousos, Biosens. Bioelectron. **24**(2), 313–318 (2008)
K. Länge, M. Rapp, Sensors Actuators B Chem. **142**, 39–43 (2009)
K. Länge, G. Blaess, A. Voigt, R. Götzen, M. Rapp, Biosens. Bioelectron. **22**(2), 227–232 (2006)
K. Länge, B.E. Rapp, M. Rapp, Anal. Bioanal. Chem. **391**(5), 1509–1519 (2008)
J. Lee, Y.S. Choi, Y. Lee, H.J. Lee, J.N. Lee, et al., Anal. Chem. **83**(22), 8629–8635 (2011)
W. Lee, J. Jung, Y.K. Hahn, S.K. Kim, Y. Lee, et al., Analyst **138**(9), 2558–2566 (2013)
D. Matatagui, D. Moynet, M.J. Fernandez, J. Fontecha, J.P. Esquivel, et al., Sensors Actuators B Chem. **185**, 218–224 (2013)
D. Matatagui, J.L. Fontecha, M.J. Fernandez, I. Gracia, C. Cane, J.P. Santos, M.C. Horrillo, Sensors **14**, 12658–12669 (2014)
G. McHale, F. Martin, M.I. Newton, J. Appl. Phys. **92**, 3368–3379 (2002)
K. Mitsakakis, E. Gizeli, Anal. Chim. Acta **699**(1), 1–5 (2011a)
K. Mitsakakis, E. Gizeli, Biosens. Bioelectron. **26**(11), 4579–4584 (2011b)
K. Mitsakakis, A. Tserepi, E. Gizeli, J. Microelectromech. Syst. **17**, 1010–1019 (2008)
K. Mitsakakis, A. Tsortos, E. Gizeli, Analyst **139**(16), 3918–3925 (2014)
G. Papadakis, E. Gizeli, Anal. Methods **6**, 363–371 (2014)
G. Papadakis, A. Tsortos, E. Gizeli, Biosens. Bioelectron. **25**(4), 702–707 (2009)
G. Papadakis, A. Tsortos, F. Bender, E.E. Ferapontova, E. Gizeli, Anal. Chem. **84**, 1854–1861 (2012)
G. Papadakis, A. Tsortos, A. Kordas, I. Tiniakou, E. Morou, J. Vontas, D. Kardassis, E. Gizeli, Sci Rep **3**, 2033 (2013)
G. Papadakis, N. Skandalis, A. Dimopoulou, P. Glynos, E. Gizeli, PLoS One **10**, e0132773 (2015)
M. Perpeet, S. Glass, T. Gronewold, A. Kiwitz, A. Malavé, et al., Anal. Lett. **39**, 1747–1757 (2006)
A. Rasmusson, E. Gizeli, J. Appl. Phys. **90**, 5911–5914 (2001)
K. Saha, F. Bender, E. Gizeli, Anal. Chem. **75**(4), 835–842 (2003)
O. Tamarin, S. Comeau, C. Déjous, D. Moynet, D. Rebière, J. Bezian, J. Pistré, Biosens. Bioelectron. **18**(5–6), 755–763 (2003)
A. Tsortos, G. Papadakis, K. Mitsakakis, K. Melzak, E. Gizeli, Biophys. J. **94**(7), 2706–2715 (2008)
A. Tsortos, A. Grammoustianou, R. Lymbouridou, G. Papadakis, E. Gizeli, Chem. Commun. **51**, 11504–11507 (2015)
A. Tsortos, G. Papadakis, E. Gizeli, Anal. Chem. **88**, 6472–6478 (2016)
I. Voiculescu, A.N. Nordin, Biosens Bioelectron **33**, 1–9 (2012)
J. Wu, Z. He, Q. Chen, J.-M. Lin, Trac-Trend Anal Chem **80**, 213–231 (2016)